

# Imaging with extended focal depth by means of the refractive light sword optical element

J. Ares García<sup>1</sup>, S. Bará<sup>2</sup>, M. Gomez García<sup>2</sup>, Z. Jaroszewicz<sup>3,4</sup>, A. Kolodziejczyk<sup>5\*</sup>, and K. Petelczyc<sup>5</sup>

<sup>1</sup>*Departamento de Física Aplicada, Facultad de Ciencias, Universidad de Zaragoza, 50009 Zaragoza, Spain*

<sup>2</sup>*Area de Óptica, E.U., Óptica e Optometría, Universidade de Santiago de Compostela, 15782 Santiago de Compostela, GALIZA (Spain)*

<sup>3</sup>*Institute of Applied Optics, Kamionkowska 18, 03-805 Warsaw, Poland*

<sup>4</sup>*National Institute of Telecommunications, Szachowa 1, 04-894 Warsaw, Poland*

<sup>5</sup>*Faculty of Physics, Warsaw University of Technology, Koszykowa 75, 00-662 Warsaw, Poland*

\*Corresponding author: [kolodz@if.pw.edu.pl](mailto:kolodz@if.pw.edu.pl)

**Abstract:** The paper presents first experiments with a refractive light sword optical element (LSOE). A refractive version of the LSOE was prepared in photoresist by gray scale photolithography. Then we examined chromatic aberrations of the produced element and compared them with those corresponding to two different lenses. For this purpose we performed two experiments, the first one where white light illumination was used and the latter one by the help of monochromatic illumination with three different wavelengths. The obtained results lead to the conclusion that the refractive LSOE does not exhibit significant chromatic aberrations and can be successfully used for imaging with extended depth of focus in polychromatic illumination.

©2008 Optical Society of America

**OCIS codes:** (080.2740) Geometric optics: Geometric optical design; (110.2990) Imaging systems: Image formation theory; (110.6890) Imaging systems: Three-dimensional image processing; (220.3620) Optical design and fabrication: Lens system design.

---

## References and links

1. M. Mino and Y. Okano, "Improvement in the optical transfer function of a defocused optical system through the use of shaded apertures," *Appl. Opt.* **10**, 2219-2225 (1971).
2. J. Ojeda-Castaneda, P. Andres, and A. Diaz, "Annular apodizers for low sensitivity to defocus and to spherical aberration," *Opt. Lett.* **11**, 487-489 (1986).
3. J. Ojeda-Castaneda, E. Tepichin, and A. Diaz, "Arbitrary high focal depth with a quasioptimum real and positive transmittance apodizer," *Appl. Opt.* **28**, 2666-2670 (1989).
4. J. Ojeda-Castaneda and L. R. Berriel-Valdos, "Zone plate for arbitrarily high focal depth," *Appl. Opt.* **29**, 994-997 (1990).
5. E. R. Dowski, Jr. and W. T. Cathey, "Extended depth of field through wave-front coding," *Appl. Opt.* **34**, 1859-1866 (1995).
6. S. Bradburn, W.T. Cathey, and E.R. Dowski, Jr., "Realizations of focus invariance in optical-digital systems with wave-front coding," *Appl. Opt.* **36**, 9157-9166 (1997).
7. H. B. Wach, E. R. Dowski, Jr., and W. T. Cathey, "Control of chromatic focal shift through wave-front coding," *Appl. Opt.* **37**, 5359-5367 (1998).
8. S. C. Tucker, W.T. Cathey, and E. R. Dowski, Jr., "Extended depth of field and aberration control for inexpensive digital microscope systems," *Opt. Express* **4**, 467-474 (1999).
9. S. S. Sherif, W. T. Cathey, and E. R. Dowski, "Phase plate to extend the depth of field of incoherent hybrid imaging systems," *Appl. Opt.* **43**, 2709-2721 (2004).
10. N. Davidson, A. A. Friesem, and E. Hasman, "Holographic axilens: high resolution and long focal depth," *Opt. Lett.* **16**, 523-525 (1991).
11. B.-Z. Dong, J. Liu, B.-Y. Gu, and G.-Z. Yang, "Rigorous electromagnetic analysis of a microcylindrical axilens with long focal depth and high transverse resolution," *J. Opt. Soc. Am. A* **18**, 1465-1470 (2001).
12. J.-S. Ye, B.-Z. Dong, B.-Y. Gu, G.-Z. Yang, and S.-T. Liu, "Analysis of a closed-boundary axilens with long focal depth and high transverse resolution based on a rigorous electromagnetic theory," *J. Opt. Soc. Am. A* **19**, 2030-2035 (2002).

13. F. Di, Y. Yingbai, J. Guofan, and W. Minxian, "Rigorous concept for the analysis of diffractive lenses with different axial resolution and high lateral resolution," *Opt. Express* **17**, 1987-1994 (2003).
14. J. Lin, J. Liu, J. Ye, and S. Liu, "Design of microlenses with long focal depth based on general focal length function," *J. Opt. Soc. Am. A* (to be published).
15. J. Ares, R. Flores, S. Bara, and Z. Jaroszewicz, "Presbyopia compensation with a Quartic Axicon," *Optometry and Vision Sc.* **82**, 1071-1078 (2005).
16. J. Sochacki, A. Kołodziejczyk, Z. Jaroszewicz, and S. Bara, "Nonparaxial design of generalized axicons," *Appl. Opt.* **31**, 5326-5330 (1992).
17. J. Sochacki, Z. Jaroszewicz, L.R. Staroński, and A. Kołodziejczyk, "Annular-aperture logarithmic axicon," *J. Opt. Soc. Am. A* **10**, 1765-1768 (1993).
18. W. Chi, and N. George, "Electronic imaging using a logarithmic asphere," *Opt. Lett.* **26**, 875-877 (2001).
19. M. A. Golub, V. Shurman, and I. Grossinger, "Extended focus diffractive optical element for Gaussian laser beams," *Appl. Opt.* **45**, 144-150 (2006).
20. G.-m. Dai, "Optical surface optimization for the correction of presbyopia," *Appl. Opt.* **45**, 4184-4195 (2006).
21. A. Flores, M. R. Wang, and J. J. Yang, "Achromatic hybrid refractive-diffractive lens with extended depth of focus," *Appl. Opt.* **43**, 5618-5630 (2004).
22. Z. Liu, A. Flores, M. R. Wang, and J. J. Yang, "Diffractive infrared lens with extended depth of focus," *Opt. Eng.* **46**, 018002 (1-9) (2007).
23. J. Campos, J. C. Escalera, O. Lopez-Coronado, R. Gimeno and M. J. Yuzuel, "Depth of focus increase by multiplexing programmable diffractive lenses," *Opt. Express* **14**, 10207-10219 (2006).
24. E. E. Garcia-Guerrero, E. R. Mendez, H. M. Escamilla, T. A. Leskova, and A. A. Maradudin, "Design and fabrication of random phase diffusers for extending the depth of focus," *Opt. Express* **15**, 910-923 (2007).
25. G. Mikula, Z. Jaroszewicz, A. Kołodziejczyk, K. Petelczyc and M. Sypek, "Imaging with extended focal depth by means of lenses with radial and angular modulation," *Opt. Express* **15**, 9184-9193 (2007).
26. D. Mas, J. Espinosa, J. Perez and C. Illueca, "Three dimensional analysis of chromatic aberration in diffractive elements with extended depth of focus," *Opt. Express* **15**, 17842-17854 (2007).
27. A. Kołodziejczyk, S. Bara, Z. Jaroszewicz, and M. Sypek, "The light sword optical element – a new diffraction structure with extended depth of focus," *J. Mod. Opt.* **37**, 1283-1286 (1990).
28. G. Mikula, A. Kołodziejczyk, M. Makowski, C. Prokopowicz, and M. Sypek, "Diffractive elements for imaging with extended depth of focus," *Opt. Eng.* **44**, 058001(1-7) (2005).
29. J. W. Goodman, *Introduction to Fourier Optics* (McGraw-Hill, 1968), Chap. 6.

## 1. Introduction

The increased depth of focus can be a valuable advantage of incoherent imaging systems in many applications. The extended focal depth is especially important when three-dimensional scenes or three-dimensional objects should be properly imaged. Hence one can note in recent years a growing number of scientific publications devoted to this subject. The authors of these works attempted to solve the problem of the extended depth of focus in different ways and by help of different methods. Amplitude apodization can increase the focal depth [1-4] but this approach causes a substantial loss of the incident light energy and diminishes the effective aperture of the system limiting the resolution of imaging. The two step process based on the use of a proper phase filter in an optical set-up and a further electronic processing was applied successfully in microscopy [5-9]. Nevertheless the second electronic stage of this approach makes impossible to use the method for imaging in real time.

Especially well suited for real time imaging with extended focal depth seem to be optical elements focusing light into line focal segments. From a theoretical point of view they are equivalent to lenses with properly controlled aberrations. A focus stretched in the form of a line segment hereby makes possible to connect a certain range of input object planes with a certain range of output image planes according to the lens equation. The elements of this kind can be designed in different ways including geometrical approach [10-15], the ray tracing method completed by the energy conservation principle [16-19], iterative methods [20-22] or stochastic methods [23, 24]. All these elements besides the structures obtained by stochastic methods exhibit symmetry of revolution, i.e., their transmittances depend only on the radial coordinate in the polar system. Lately we have presented numerical and experimental results concerning the optical properties of the light sword optical element (LSOE) where additionally an angular modulation of a transmittance was implemented [25]. Our work pointed out to the superiority of the diffractive LSOE over the other diffractive elements with radial modulation of the transmittance only, at least in an optical set-up simulating a human

eye. Nevertheless diffractive elements including those focusing light in a line segment suffer from substantial chromatic aberrations. This effect reveals especially in a case of the diffractive LSOE forming at the same plane well separated output focal spots corresponding to different wavelengths [26]. Strong chromatic aberrations of the diffractive LSOE limit practically its imaging applications to monochromatic cases. Hence the only reasonable solution to this problem when polychromatic or white light illumination is used seems to be the substitution of the diffractive element by its refractive counterpart.

This paper presents first imaging experiments with the refractive LSOE. Our goal was an experimental study of chromatic aberrations of this element in an imaging set-up with white light illumination. For a better illustration we have compared the imaging properties of the refractive LSOE with those corresponding to two lenses with a similar numerical aperture. In the Section 2 we give the theoretical background describing the design of the LSOE and its focusing properties. Section 3 presents the experimental results. The last Section discusses the results of the experiments of the refractive LSOE.

## 2. Theoretical background

The LSOE is a thin optical element, whose phase transmittance has the following form in the polar coordinate system:

$$\Phi(r) = -\frac{kr^2}{2[f_1 + (\Delta f \theta / 2\pi)]}, \quad (1)$$

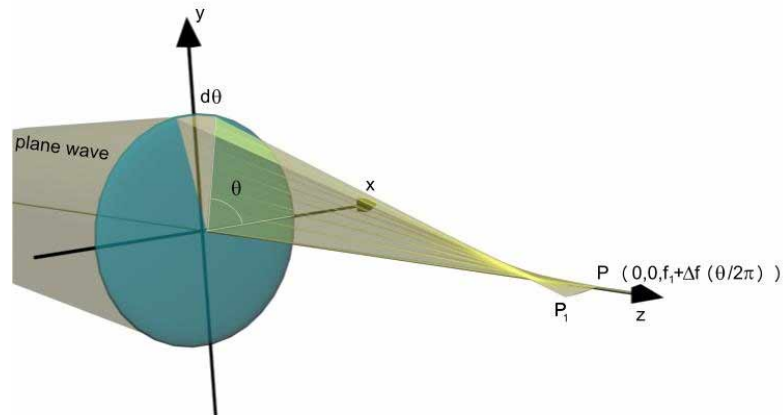


Fig. 1. Scheme of focusing by the LSOE under plane wave illumination. The infinitesimal angular sector of the element focuses an incident plane wave into a segment  $PP_1$  oriented perpendicularly to the sector.

where  $r$ ,  $\theta$  are respectively the radial and azimuthal coordinates;  $k=2\pi/\lambda$  and  $\lambda$  is the wavelength of light. For a fixed value of the angular argument  $\theta$  the phase transmittance  $\Phi(r)$  is equivalent to that of a thin lens with focal length  $f_1 + \Delta f \theta / 2\pi$ . Therefore in a first approximation the LSOE focuses an incident plane wave into a focal segment of width  $\Delta f$ . When  $\theta \in [0, 2\pi)$  then the segment is stretched from a distance  $f_1$  to a distance  $f_1 + \Delta f$  behind the LSOE plane. A more detailed analysis leads to a conclusion that the element described by Eq. (1) forms approximately an assumed focal segment even within the geometrical optics. According to the paraxial ray tracing implemented to polar coordinates points  $(r, \theta)$  of the infinitesimal angular sector  $\theta=\text{const}$  of the element are connected to the following points  $(\rho, \varphi)$  of the output plane  $z = f_1 + \Delta f \theta / 2\pi$ :

$$\rho = r\Delta f / (4\pi f_1 + 2\Delta f\theta), \quad \varphi = \theta + \pi/2. \quad (2)$$

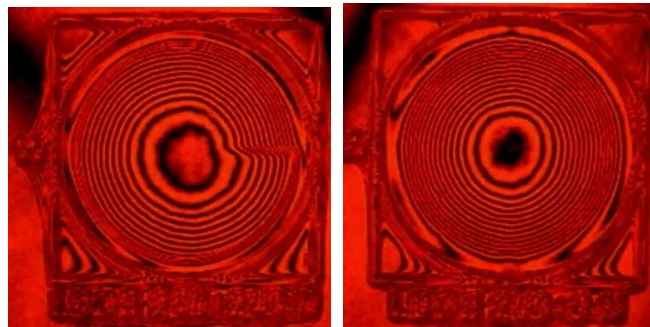
The geometry of light focusing by the LSOE according to the ray tracing method is shown in Fig. 1. The infinitesimal angular sector of the element corresponding to the angular coordinate  $\theta$  focuses light into a small line segment  $PP_1$  instead into an assumed point P with coordinates  $(0,0, f_1 + \Delta f\theta / 2\pi)$  in the Cartesian coordinate system OXYZ.

A superiority of the diffractive LSOE for imaging with extended focal depth over lenses, axilenses and axicons was already proven numerically and experimentally [25, 27, 28]. A new concept of angular modulation of transmittance seems to be effective. Surprisingly good abilities of the LSOE for imaging with extended depth of field are probably connected with the flow of energy during focusing. According to ray tracing illustrated in Fig. 1, the focusing process has an off-axis character. The maximum intensity of the focal spot lies outside the optical axis OZ and waves around it [28]. This phenomenon causes a displacement of the output images. The flow of energy changes its main direction during focusing and positions of output images rotate around the optical axis. Then the effect of mutual disturbance between neighboring images corresponding to different focal lengths or different object distances is less harmful than in cases of elements with symmetry of revolution where the flow of energy during focusing has the same main direction along the optical axis. In consequence the output focal spots, point spread functions and modulated transfer functions corresponding to the LSOE almost conserve their shape and character for a wide range of defocusing parameters [25, 28]. Therefore the LSOE with an angular modulation of its transmittance can exhibit its superiority for imaging with extended depth of focus over optical elements with symmetry of revolution where controlled spherical aberration is used. Nevertheless, the increased depth of focus comes at a cost. The LSOE exhibits some disadvantages. It forms slightly stretched focal spots without radial symmetry [28] what generates characteristic blur of output images. These images wave around the optical axis. The above disadvantages do not seriously limit usefulness of the LSOE for many imaging applications. According to the already presented results the diffractive LSOEs of moderate numerical apertures can be at least used successfully in machine vision and ophthalmologic applications [25].

Unfortunately, a diffractive LSOE can be used for imaging purposes only in monochromatic illumination what substantially limits possible applications especially in ophthalmology. As was shown lately the off-axis focusing corresponding to the LSOE generates strong chromatic aberrations [26]. The focal spots formed by different wavelengths are considerably mutually shifted in the same output plane. Then one can expect a poor quality of imaging when polychromatic or white light will be used. In order to avoid this serious drawback the LSOE can be fabricated in a thin refractive version. Chromatic aberrations of refractive elements are one order of magnitude smaller than diffractive ones or even more. Assuming that the refractive index is independent on the light frequency, the form of the phase transmittance given in Eq. (1) remains the same for the different wavelengths  $\lambda$  of visible light.

### 3. Experiment

The refractive elements were produced by gray scale photolithography of sol-gel photoresist deposited onto 1 mm thick circular glass substrates of 25.4 mm diameter. In this way we have fabricated two elements, the LSOE and a spherical lens for a comparison in an imaging set-up. The maximum height of the refractive profile of our elements was 20  $\mu\text{m}$  (peak-to-valley). Fig. 2 presents interferograms of the refractive LSOE and the refractive lens in a Mach-Zender interferometer. According to these interferograms the refractive structures exhibit a certain amount of spherical aberration caused by imperfections in the fabrication process, mainly due to the limited number of gray levels printable on gray scale mask, which was equal to 256. Both elements had a circular aperture of diameter 4.7 mm. Then we measured the focal parameters of the LSOE and the lens in an optical set-up. We obtained a focal length of the lens equal to  $f_2=28.5$  cm and the parameters  $f_1=30$  cm,  $\Delta f=15$  cm corresponding to the LSOE.



(a)

(b)

Fig. 2. Interferograms of the fabricated LSOE (a) and the lens (b) obtained in a Mach-Zender interferometer.

Afterwards we performed two experiments illustrating the chromatic properties of the refractive LSOE. In all cases the input object consisted of four Snellen optotypes. Each optotype had the form of a properly oriented capital E with 2 mm height and a smallest detail of 0,4 mm. The input object was placed at a fixed distance 70 cm in front of the imaging element and the distance of the image plane behind the element was changed. According to the lens equation and the parameters given above the fabricated LSOE was designed to form output images lying in planes distant from 52.5 cm up to 126 cm what corresponds to defocusing 1.1 D measured in optical power.

During the first experiment we used as input objects a positive and a negative of the Snellen optotypes illuminated by the white light emitted by an ordinary filament lamp of power 35 W. Additionally we compared the imaging properties of the fabricated elements with those of a professional Carl Zeiss objective of focal length  $f_2=30$  cm. In order to have comparable numerical apertures we reduced the circular aperture of the objective to a diameter of 5 mm. The experimental results for different defocusing parameters are presented in Fig. 3 in form of color photographs. The defocusing, given in optical power, was calculated separately for each element according to the formula  $1/f-1/p-1/q$ , where  $f$ ,  $p$ ,  $q$  denote the focal length of the element, the object distance and the image distance respectively. In case of the LSOE we assumed that  $f=f_1$ . The experiment illustrates well the achromatic character of imaging realized by the refractive LSOE. The photographs make impression to be prepared in a gray-scale. No color is clearly visible except white, black and gray. What is most important, the refractive LSOE similarly to its diffractive version exhibits distinctly abilities for imaging with extended depth of focus. Images of optotypes formed by the LSOE are readable in a presented range of defocusing 0D – 1D, otherwise to images created by lenses which are considerably blurred for substantial defocusing. One can observe that the focal depth of the spherical lens fabricated on photoresist is significantly bigger than that of the professional objective, because of the residual spherical aberration present in the former.

The main purpose of the paper is an illustration and an analysis of chromatic aberrations of a refractive LSOE and not a comparison of focal depths realized by the LSOE and the lenses. As we have already pointed out, a superiority of the LSOE for imaging with increased focal depth of focus over elements with symmetry of revolution was shown before [25, 27, 28]. Therefore we present in Fig. 3 output images created by lenses corresponding to only positive values of the defocusing. It is necessary to take into account that lenses can realize readable images also in a case of small negative values of the defocusing. On the other hand according to the paraxial theory of lenses the optical transfer function is an even function of the used defocusing parameter [29]. Hence in a case of negative defocusing values one can expect quality of images similar to these created by lenses and shown in Fig. 3.

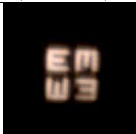

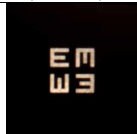





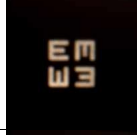
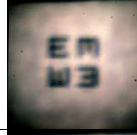
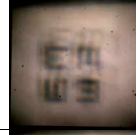



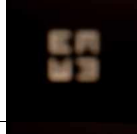
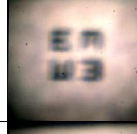


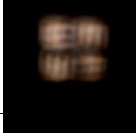


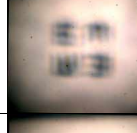

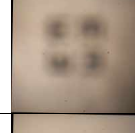
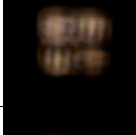


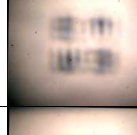
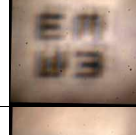










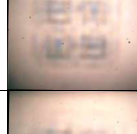
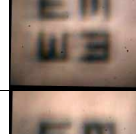




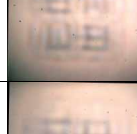
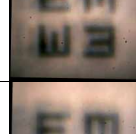

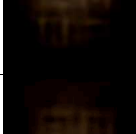

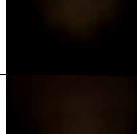


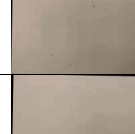
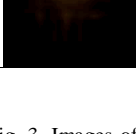
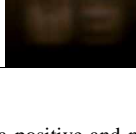


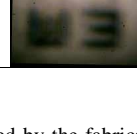
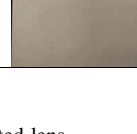
	LENS (f=28,5cm)	LSOE (f=30-45cm)	OBJECTIVE (f=30cm)	LENS (f=28,5cm)	LSOE (f=30-45cm)	OBJECTIVE (f=30cm)
0 D						
0,11 D						
0,22 D						
0,33 D						
0,44 D						
0,55 D						
0,66 D						
0,77 D						
0,88 D						
1 D						

Fig. 3. Images of a positive and negative of Snellen optotypes formed by the fabricated lens, the LSOE and the objective in a case of different defocusing parameters given in optical power.

In order to illustrate the experimental results more completely we present in Fig. 4 images formed by the refractive LSOE in the full range of defocusing from 0D to 1D, corresponding to image distances from 52.5 cm to 110,5 cm.

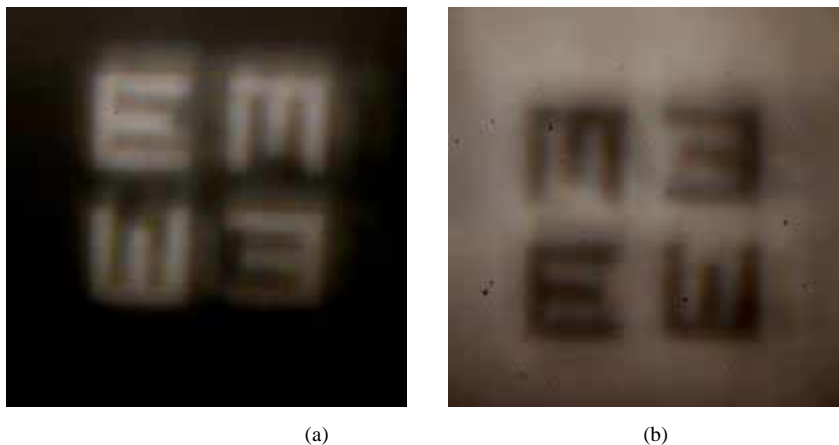


Fig. 4. Images of a positive ([Media 1](#), 181 kB) and negative ([Media 2](#), 217 kB) of the Snellen optotypes formed by the LSOE and corresponding to the full range of analyzed defocusing from 0D to 1D.

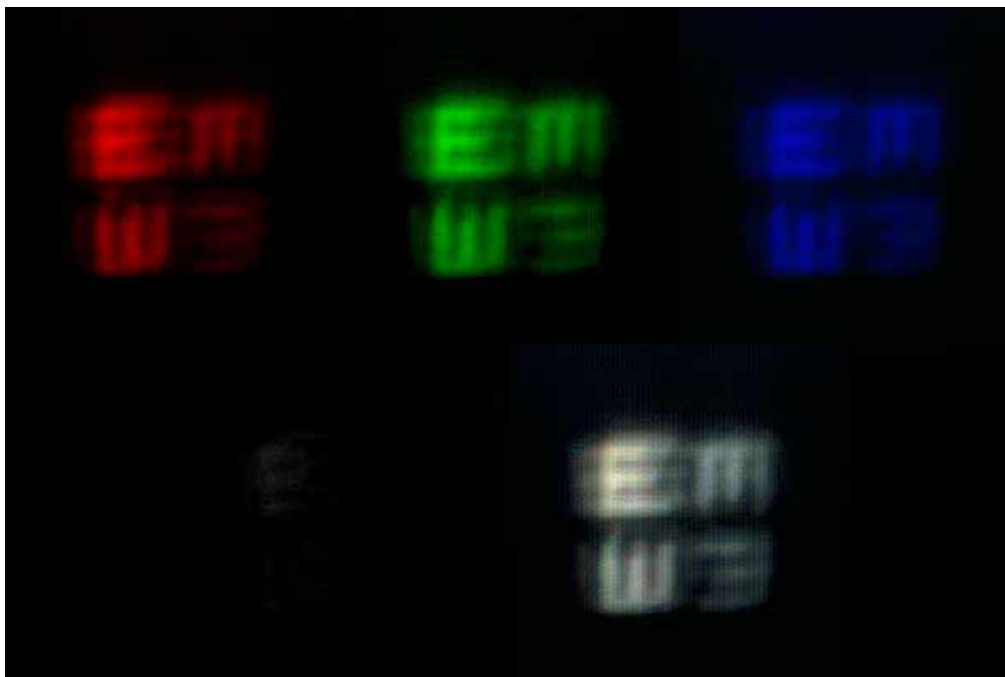


Fig. 5. Images of Snellen optotypes formed by the LSOE in red, green and blue monochromatic illumination ([Media 3](#), 692 kB). Details of the figure are given in the text.

For a more detailed analysis of the chromatic properties of the fabricated LSOE we performed the second experiment with a positive of the Snellen optotypes as input object. The



object was in turn illuminated through a rotating ground-glass by monochromatic light with the following wavelengths:  $\lambda_1=632.8$  nm (red),  $\lambda_2=514.4$  nm (green),  $\lambda_3=458$  nm (blue). For a fixed wavelength the image distance  $q$  belonged to the same range [27.5 cm; 87.5 cm]. We present in Fig. 5 the experimental results corresponding to the full range of the examined defocusing. The upper row in Fig. 5 shows the normalized intensity of images formed in red (R), green (G) and blue (B) light at the same output plane corresponding to a fixed image distance  $q$ . The sum of these three images realized by particular RGB channels is presented on the right side of the bottom row in Fig. 5. In the same row on the left side one can see the subtraction of the normalized intensities of R and B images from the upper row.

The second experiment confirms the achromatic character of images formed by the refractive LSOE. R, G, B images have the same size and occupy the same position in the output plane. Their sum result in a gray-scale pattern and the subtraction of R and B images leads to an almost zero output bitmap.

#### 4. Conclusions

We presented experiments illustrating the imaging properties of the refractive LSOE. According to the previous publications the diffractive LSOE can be successfully applied for imaging with extended depth of focus [25, 27, 28]. Unfortunately this element exhibits strong chromatic aberrations that limit its practical use only for a monochromatic illumination [26]. Therefore the main aim of this work was to examine the chromatic aberrations of the refractive LSOE. For this purpose we fabricated the refractive LSOE by means of gray scale photolithography. Then two experiments were performed. Both gave evidence that chromatic aberrations of the refractive LSOE are sufficiently small in order to not to disturb visually imaging in a white light. Therefore one can expect that the diffractive LSOE can be successfully substituted in polychromatic light by its refractive counterpart for those applications where imaging with extended depth of focus is desirable.

#### Acknowledgments

This work was supported by Warsaw University of Technology, by National Institute of Telecommunications and by the Spanish Ministerio de Educación y Ciencia, Plan Nacional de Investigación Científica, Desarrollo e Innovación Tecnológica (I+D+i), grant FIS2005-05020-C03-02 and FEDER.

We would like to thank our referee for valuable remarks which helped us to clarify the paper.